SAND2019-0213C

Proceedings of the 2019 Hypervelocity Impact Symposium
HVIS2019
April 14-19, 2019, Destin, FL, USA
HVIS2019-XXX

Mesoscale modeling and debris generation in hypervelocity impacts

Stephanie N. Q. Bouchey* and Jeromy T. Hollenshead

Sandia National Laboratories, PO Box 5800 Mail Stop 1185, Albuquerque, NM 87185-1185

Abstract

Material fragmentation after a hypervelocity impact is of interest to predictive electro-optical and infrared (EO/IR) modeling. Successful comparisons with data require that submicron fragments are generated in such impacts; however, experimental data has so far been unable to produce fragments of this scale. The purpose of this work was therefore to investigate the generation of debris in hypervelocity impacts through sphere-on-plate simulations with the shock physics code, CTH. Specifically, it tested the effect of explicitly modeling the mesoscale grain structure in aluminum with the use of two suites of simulations. The first suite tested the standard isotropic/homogeneous structure and the second study explicitly modeled mesoscale grains and tested the effect on fragment size through the proxy of Grady-Kipp strain rate at failure and material temperature. The isotropic model highlighted findings that demonstrate the underlying physics of the hypervelocity impact problem, whereas the mesoscale grain model explored the effect and sensitivity of a range of key material properties within the grain structure. Comparisons were made between the two simulation suites primarily using histograms and cumulative mass plots of Grady-Kipp strain rate at failure and material temperature. Attempts to change material properties or interface behavior between grains had only a minor effect. Material porosity was the only study to demonstrate an exceptional change in both the Grady-Kipp strain rate at failure and material temperature, but high levels of porosity were used. Shock reflections from voids induced higher strain rates and material temperatures, and similar effects may be produced from inclusions or dislocations in real materials. Thus, interfaces within a material, such as those caused by porosity may play a role in producing smaller debris fragments that support the EO/IR predictive models of flight test data.

Keywords: debris generation, mesoscale grain structure, EO/IR modeling, CTH, Grady-Kipp strain rate at failure

1. Introduction

This effort investigated the generation of debris in hypervelocity impacts of a sphere on a flat, semi-infinite plate. It is hypothesized that explicit modeling of grains, especially in the presence of void and varying grain properties, may lead to differences in predicted strain rates (locally higher) associated with the grain boundaries. Such an effect may lead to smaller predicted fragments sizes than when using the traditional isotropic/homogeneous modeling approach and may provide improved understanding of modeling fragmentation in hypervelocity impacts. In addition, results of this study may help provide evidence supporting the generation of sub-micron fragments currently required by many electro-optical and infrared (EO/IR) predictive models to successfully compare with observed flight test data.

Two suites of simulations comprised this study. First, the Isotropic Study focused on the underlying impact physics in the traditional isotropic (homogeneous) continuum approach. Results from the Isotropic Study served as a baseline and point of comparison to the second simulation suite, which explicitly modeled the mesoscale grain structure. Such an approach allowed various changes to the structure and properties to be made, which enabled the investigation of solution sensitivity to a range of key parameters including varying the projectile size, computational mesh resolution, explicit modeling of grains, and modifying

* Corresponding author. Tel.: +1-505-284-8128
E-mail address: snquint@sandia.gov

material properties. Comparisons between the two studies were made on predicted strain rates at failure and material temperature, both of which were used as proxies for fragment sizes.

2. Input development

Computational modeling was performed at Sandia National Laboratories using the shock physics analysis package, CTH [1-2]. The current investigation is based on two-dimensional (2D) descriptions of the problem. In order to compare the two different modeling approaches, two designs were required. The first used the traditional isotropic macro-scale description of the materials, in which both the target and impactor were represented as two separate, bulk materials. The nominal problem design was sphere impacting a semi-infinite flat plate target at a nominal velocity of 4 km/s. The projectile was modeled as a sphere of Aluminum 1100 with the SESAME equation of state, a Johnson-Cook viscoelastic strength model, a Johnson-Cook fracture model, and a Grady-Kipp fragmentation model. A fracture/spall pressure of 124 MPa was also used. The target was modeled as a semi-infinite flat plate of Aluminum 7075, also with the SESAME equation of state, Johnson-Cook strength, Johnson-Cook fracture, and Grady-Kipp fragmentation. In the target, a fracture/spall pressure of 575 MPa was used. The small differences between the target and projectile materials were based on previous, similar simulations and provided some contrast between the two materials.

Although the isotropic model was developed first, many of the system characteristics (e.g. resolution, problem geometry) were driven by the expected requirements for the mesoscale model description. For example, it was nominally desired that the grains in the mesoscale simulations have at least 4 cells across their diameter. This requirement led to a nominal flat mesh resolution of 3.5 µm, but such high resolution necessitated exceptionally small simulation domains to incorporate the sphere-on-plate geometry. Initial studies evaluated the effects associated with four different impactor diameters: 7 mm, 3.5 mm, 1.4 mm, and 0.7 mm (corresponding to 500 grains, 250 grains, 100 grains, and 50 grains across the impactor, respectively). To reduce edge and boundary effects, the target was designed to be much larger than the projectile. The total target area was 2.1 cm wide by 4.1 cm deep. However, the computational expense of filling this entire area with grains would be prohibitive. A smaller "grains region" of the target was modeled to be 3.5 mm thick and 7 mm wide (14 mm wide when mirrored about the axis). In the isotropic design, this small target area was modeled as a single material that matched the material properties of the larger surrounding "target matrix area." In both cases the target matrix area was modeled with a single material.

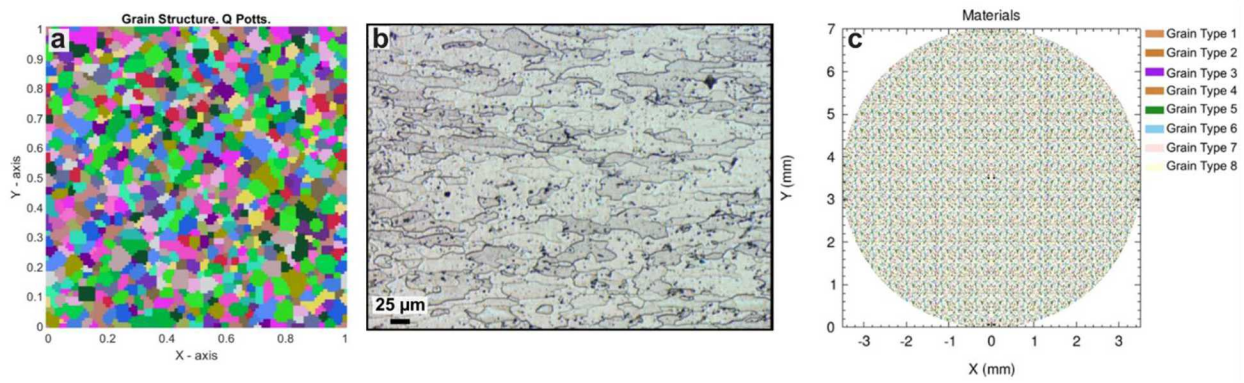

Fig. 1. A grain structure is produced in MATLAB (a) based on a pure aluminum sample [3] (b) to yield a geometry filled with grains in CTH (c).

Traditional model descriptions within CTH are typically macro-scale and do not include any explicit grain structure representation. Consequently, a procedure to model and initialize grains within CTH was necessary. A MATLAB Monte Carlo simulation of 2D grain growth using a Q-state Potts model generated a unit cell of grains. The current configuration allows for eight different grain types in both the target and projectile (16 total materials). Each grain type was randomly distributed within the unit cell, and the entire cell was then scaled such that the average grain size was ~14 µm in diameter, a size characteristic of aluminum estimated from Nakai and Itoh (2014) [4]. Typically, after surface treatments, the grains are stretched in one direction and do not have a 1:1 aspect ratio. The value of 14 µm was selected based on the short axis of an aluminum grain. Finally, this

scaled unit cell was tiled repeatedly to generate the impact geometry (projectile and target grains areas), and the result was written out pixel by pixel in a form (diatom) that could be read by CTH (Fig. 1).

3. Isotropic Model

The isotropic model suite simulated a projectile striking a target within a larger target matrix. This model suite enabled the following studies: resolution, impact velocity, projectile size, and projectile shape. A custom post-processing script produced cumulative distribution functions (CDFs) and histograms for Grady-Kipp strain rate at failure and material temperature.

3.1. Resolution Study

For the resolution study, a single projectile size (1.4 mm diameter) was evaluated across a range of resolutions: 14.0, 7.0, 3.5, 1.75, and 0.875 µm. The impact velocity was 4 km/s. Across all resolutions, material temperature appeared to be converged but not the strain rate at failure. Higher resolution projectiles exhibited higher strain rates with a wider overall strain rate distribution. Rise time of the initial peak in strain rate did converge for resolutions higher than 14 µm. Based on these results, the 14 µm resolution mesh was excluded from the rest of the study. Similar plots for the target revealed less variation in strain rate and little to no bimodality, indicating that a property of the projectile (size, geometry), rather than of the material, was likely causing the variation in strain rate between resolutions. These results prompted a size and geometry study.

3.2. Projectile Size Study

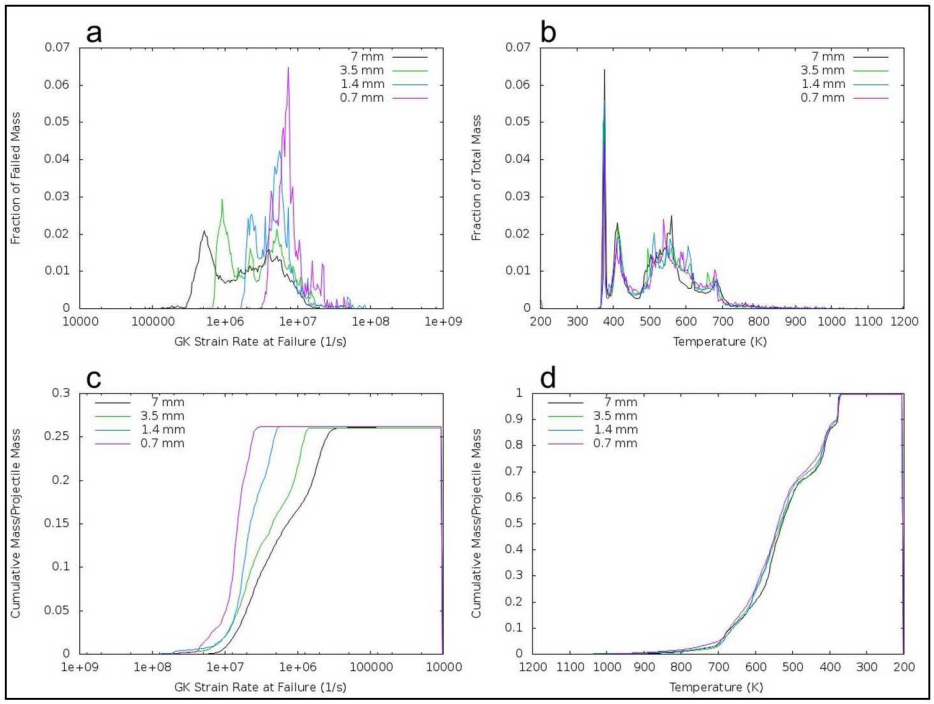

Fig. 2. Projectile Size Study Results. Histograms for (a) Grady-Kipp strain rate at failure and (b) material temperature compared to equivalent scaled cumulative mass plots of (c) Grady-Kipp strain rate at failure and (d) material temperature. Note that the axes are reversed for the cumulative mass plots.

The projectile size study tested the effects of projectile curvature and overall size relative to the domain. Histograms and CDFs were evaluated at equivalent times for each model, which was the time at which the projectile would travel one projectile diameter into the target based only on projectile speed. The histograms and CDF plots for strain rate at failure and temperature are shown in **Error! Reference source not found.** for the projectile. Material temperature was similar between all projectile sizes. This surprising temperature effect seems to be related to geometry scaling. Even though the projectile imparted more kinetic energy

with increasing size, the volume of affected material also increased. Conversely, Grady-Kipp strain rate at failure varied significantly between projectile sizes, with smaller projectiles manifesting higher strain rates in both the projectile and the target. In the projectile, the histogram of strain rate at failure exhibited a bimodal shape. The distance between the peaks in each strain rate histogram may be at least partially driven by transit time across the object (i.e., by a characteristic length scale, which is projectile diameter in this case). In the semi-infinite target, the strong bimodality seen in the projectile was absent, which suggests that the bimodality may be due primarily to projectile shape. In both the projectile and target, however, onset of the strain rate histogram was related to projectile size. Experiments and application of this study will likely use larger projectiles than those described here; therefore, the largest projectile size (7 mm) was used in the grain-modeling suite (Section 4).

3.3. Projectile Shape Study

Three additional simulations tested projectile shape by impacting a cube (face-on), rather than a sphere, into the target. Results for the projectile are shown in Fig. 3. The lack of bimodality in **Error! Reference source not found.**a is evidence that bimodality is a product of projectile curvature (as was suggested in the previous projectile size study). A more step-like strain rate at failure histogram was apparent, especially in the larger cube impacts. The size of the cube, however, did not influence temperature; this result was also seen in the sphere impacts. Histograms like those obtained for the projectile in this study are expected for finite-thickness targets (plates). The results in the semi-infinite target in this study are comparable to those from the projectile size study above, which indicates that projectile shape is less important than size when studying the target response.

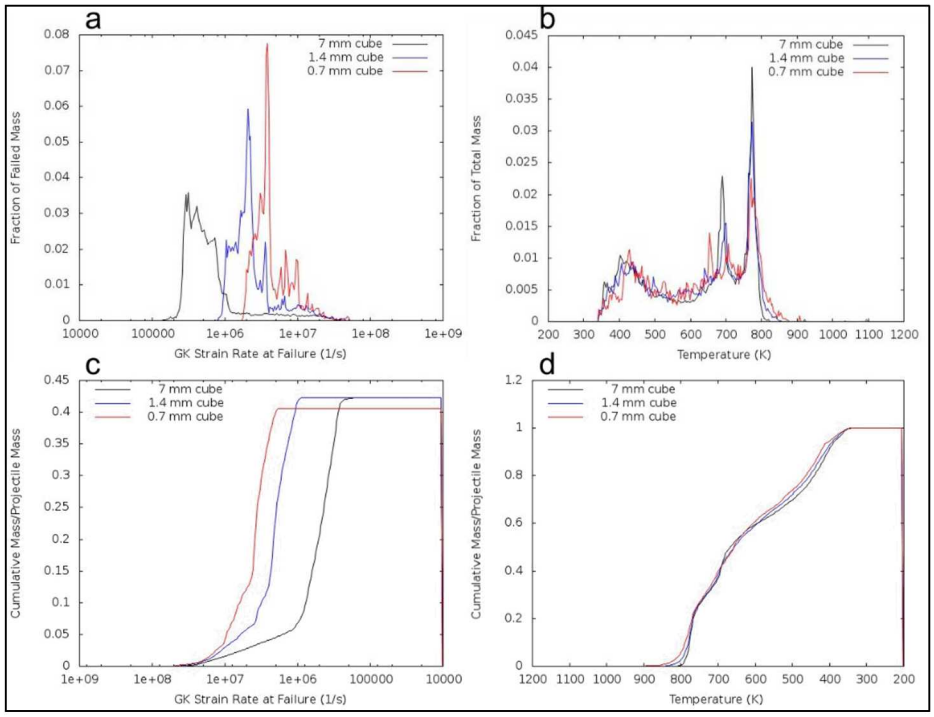

Fig. 3. Projectile Shape Study. Histograms for (a) Grady-Kipp strain rate at failure and (b) material temperature compared to equivalent scaled cumulative mass plots of (c) Grady-Kipp strain rate at failure and (d) material temperature for three different projectile sizes.

3.4. Impact Velocity Study

Finally, an impact velocity study demonstrated the effect of increasing impact velocity from the nominal 4 km/s to 6 km/s. Increases in impact velocity resulted in a shift to higher strain rates and temperatures, but overall shape and bimodality (in the projectile) were not significantly affected. Impact velocity clearly controls temperature in the projectile, although temperature

histograms were nearly unchanged by projectile size for impacts at the same speed. The rest of the simulations were performed at the nominal 4 km/s.

4. Mesoscale Model

In the mesoscale model, the projectile and "grains region" of the target were filled with individual grains, which were described in CTH as separate materials. Eight grain types were randomly distributed through the projectile by the tile method described in Section 2. Similarly, eight (separate) grain types were randomly distributed and tiled through the target grains region. The surrounding target matrix was defined as a single material. This modeling approach enabled the following studies: fracture strength distribution, yield strength distribution, slip interfaces, and porosity. A separate histogram and CDF was produced for each grain type, because each grain was described as separate materials. The histograms/CDF results of each grain were then averaged for ease of comparison with the isotropic simulation. An initial "consistency case" compared the isotropic simulation with a mesoscale model in which all the grains within the projectile (and also for the target) were modeled with the same material properties. Some numerical inconsistencies resulted in slight differences between the consistency and isotropic cases; therefore, results in this section will be compared to the consistency case, rather than the isotropic one.

4.1. Fracture Study

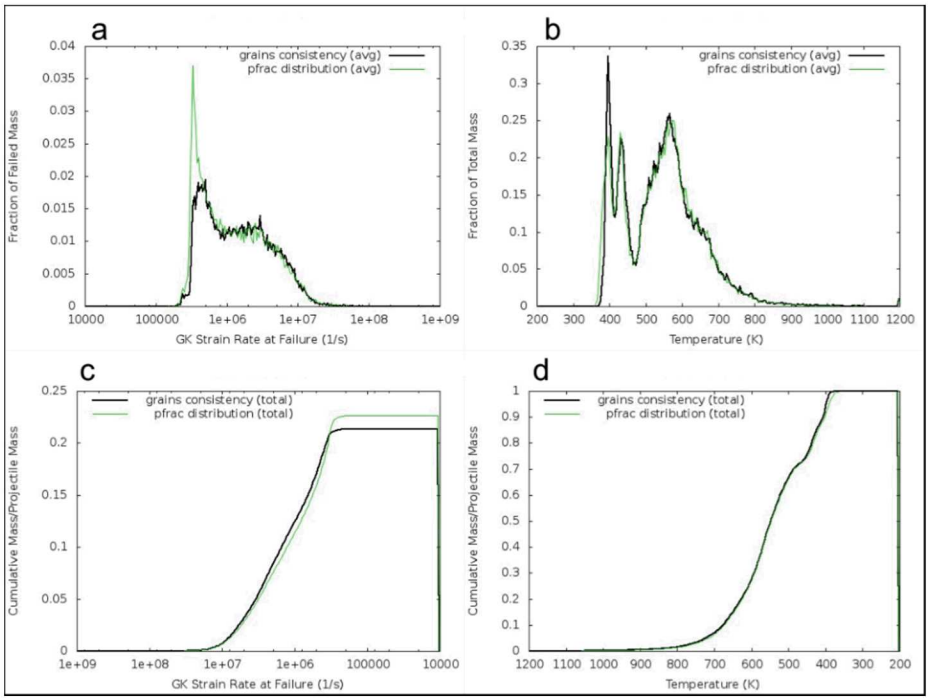

Fig. 4. Fracture Strength Study, 7-mm diameter projectile. Comparison of the grains consistency case (black line) with the results from using a fracture strength distribution in the grains. Histograms for (a) Grady-Kipp strain rate at failure and (b) material temperature compared to equivalent scaled cumulative mass plots of (c) Grady-Kipp strain rate at failure and (d) material temperature.

Fracture strength may play a role in the resulting strain rate at failure and material temperature, which ultimately affects the size of fragments produced in a hypervelocity impact. Aluminum alloys vary in fracture strength, and so to simulate this variation in the mesoscale model, a distribution of plausible fracture strengths was applied to the grains in both the projectile and the target. The distribution was centered on the fracture strength of Aluminum 1100, 5.72E+9 dyn/cm^2. Results for this study can be found for the projectile in Fig. 4. The inclusion of a fracture strength distribution within the grains resulted in an increase in the lowest strain rates compared to the grains consistency result. In the projectile, this increase in low strain rates corresponded to the first

peak in the strain rate at failure histogram. The second peak, however, remained similar between the two tests. Additionally, temperature remained largely unchanged between the fracture study results and the consistency result.

4.2. Yield Study

Yield strength also varies from one aluminum alloy to another. In CTH, the Johnson-Cook yield strength is calculated with Equation 1,

$$Y = (A + B{\varepsilon_p}^n)(1 + C \ln {\dot{\varepsilon}_p}^*)(1 - T^{*m}), \tag{1}$$

where ε_p is the equivalent plastic strain; $\dot{\varepsilon}_p$ is the plastic strain rate; T is the homologous temperature, $(T\text{-}T_{room})(T_{melt}\text{-}T_{room})$; and A, B, C, m, and n are all material constants [5-7]. The fracture strength distribution previously studied was kept for this strength investigation. A range of values for A, B, and C was found from various aluminum alloys, and normal distributions were made such that they centered on the Aluminum 1100 default values (similar to the process described in the Fracture Study above). These distributions were then incorporated into the grain-type materials of both the target and the projectile. All other values in Equation 1 remained as the Aluminum 1100 defaults.

The strength of the grains did not have a substantial effect on the second peak in the projectile strain rate histogram, nor did it have a consequential effect on material temperature (Fig. 5a-d). The first strain rate peak, however, was observed to narrow in comparison to the grains consistency test. This narrowing resulted in less material at lower strain rates, which is demonstrated by the drop in cumulative mass in the corresponding CDF. In comparison, a yield strength distribution in the target grains more significantly reduced the Grady-Kipp strain rate at failure histogram and shifted the plot to slightly higher strain rates (Fig. 5e-h). This effect resulted in less material at lower strain rates. Target material temperature was not significantly affected.

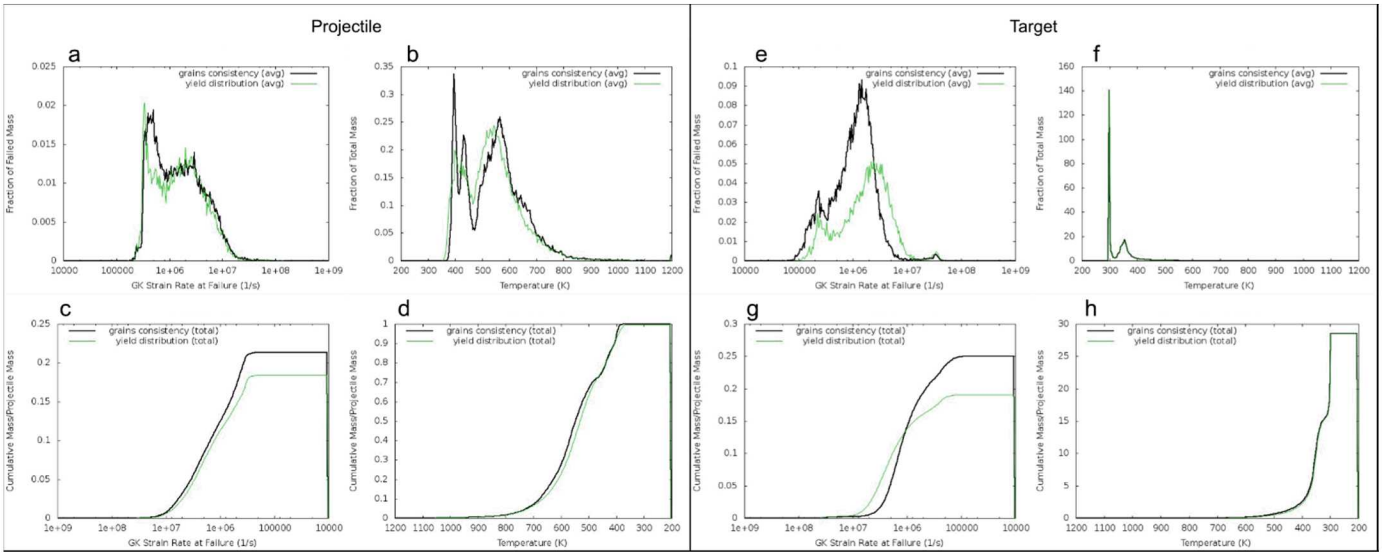

Fig. 5. Yield Strength Study, 7-mm diameter projectile. Comparison of the grains consistency case (black line) with the results from using a fracture strength distribution in the grains. Histograms for (a, e) Grady-Kipp strain rate at failure and (b, f) material temperature compared to equivalent scaled cumulative mass plots of (c, g) Grady-Kipp strain rate at failure and (d, h) material temperature. Results shown for the projectile (left plots, a-d) and the target (right plots, e-h).

4.3. Slip Study

In the cases described above, the grains were treated as if they were cemented together. The next step was to allow the grains to slide freely past one another. Two algorithms are available in CTH that allow this kind of behavior. The first is the Boundary Layer Interface (BLINT) algorithm. BLINT works on pairs of materials; one material is identified as "hard" and the other is identified as "soft." The hard material is allowed to slide past the soft material [7]. Alternatively, the SLIDE option allows two

materials to slide by one another by setting the shearing velocity gradients to zero (i.e., simulates discontinuous velocity across a sliding surface). As with BLINT, SLIDE works on pairs of materials [7]. Neither SLIDE nor BLINT had a clear, dominant effect on strain rate at failure or material temperature compared with the grains consistency test. This result is likely because the grain boundaries perfectly matched each other, which had the effect of negating any sliding boundary effect.

4.4. Porosity Study

Finally, the last suite of simulations explored the role of porosity (void space) in the grain structure of both the projectile and target. To test the upper bounds of porosity effects, all grains of a single grain-type were removed from the calculation, leaving the material with 12.5% porosity. Void space resulted in interfaces between grains, which had a significant dampening effect on the shockwave traversing the grains of the target and projectile. Void space also resulted in substantial deviation from both the isotropic and the grains consistency studies in strain rate and temperature plots (Fig. 6). The strain rate at failure histogram nearly lost its bimodal shape in the projectile and shifted to higher strain rates in both the projectile and the target. This shift indicates that the projectile size is no longer the dominant property controlling the strain rate at failure. Instead, individual grains become more important. The increase in both strain rate at failure and material temperature is likely due to the passage of several shock and rarefaction waves through the grains as they reflect off free surfaces produced by the voids. This study demonstrates that interfaces within a material, such as those caused by porosity may play a role in producing smaller debris fragments that support the EO/IR predictive models of flight test data, but large porosities like these are not likely in metals.

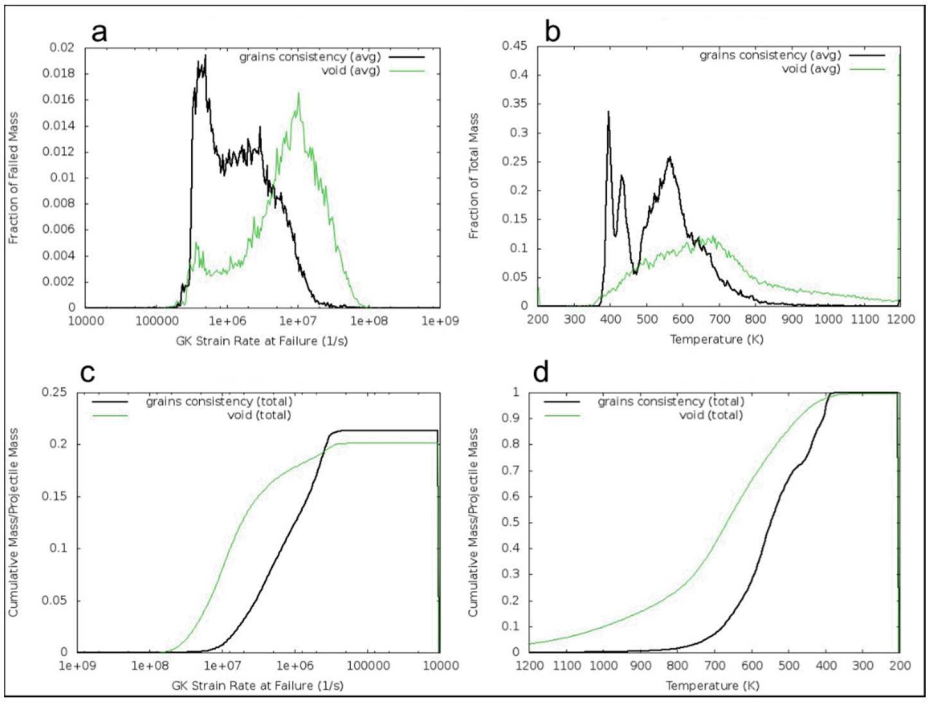

Fig. 6. Void Study, 7-mm diameter projectile. Comparison of the grains consistency case (black line) with the results from using a fracture strength distribution in the grains. Histograms for (a) Grady-Kipp strain rate at failure and (b) material temperature compared to equivalent scaled cumulative mass plots of (c) Grady-Kipp strain rate at failure and (d) material temperature.

5. Summary

This work compared the effects of modeling grain structure in hypervelocity impact simulations. Comparisons were made between a suite of simulations performed with the standard isotropic structure and one in which both the projectile and an area of the target were modeled using an accumulation of grains. Histograms and CDFs of Grady-Kipp strain rate at failure and material temperature served as a proxy for fragment size; higher temperatures and smaller strain rates result in smaller fragments.

The isotropic model was the nominal case with which the explicit modeling of grains was compared. Important findings demonstrated the underlying physics of the problem. A bimodal distribution within the projectile appeared in histograms of Grady-Kipp strain rate at failure. The onset of the first peak and the separation between the peaks was dependent on projectile size. The first peak appeared to be driven by transit time across the object (in this case, the projectile diameter), and the second peak may be related to material sound speed. The strong bimodal distribution was primarily caused by the projectile shape. A cube impacting face-on, rather than a sphere, produced a less bimodal and more stepped or punctuated histogram. Finally, velocity and projectile size had a notable effect on Grady-Kipp strain rate at failure and material temperature. Reducing the projectile size and/or increasing velocity shifted the histograms and CDFs to higher strain rates. Interestingly, for a given velocity, peak temperatures and overall temperature distributions were similar between all projectile sizes. As expected, increasing impact velocity increased material temperature.

The mesoscale model explicitly simulated a material grain structure. Important findings demonstrated the effect of the grain structure when compared to the isotropic model. Attempts to change material properties or interface behavior between grains had only a minor effect, primarily in the first peak of the Grady-Kipp strain rate histograms. Similarly, the slip study tested SLIDE and BLINT options in CTH, but neither algorithm appeared to have a consequential effect. This result is likely because the simulated grain tiles were tessellated to fit perfectly with one another. The porosity study was the only one to demonstrate an exceptional change in both the Grady-Kipp strain rate at failure and material temperature histograms and CDFs. Higher strain rates and material temperatures were observed, which resulted from shock reflections off the many free surfaces that existed because of the voids. A considerable decrease in the first strain rate histogram peak was noted, along with a complete change in histogram shape, especially in material temperature histograms.

Interfaces within a material (here, manifested as material porosity) are an important controlling factor for both strain rate and temperature during an impact. Higher strain rates and temperatures are likely to produce smaller debris fragments, which may help provide evidence supporting the generation of sub-micron fragments currently required by many EO/IR predictive models to successfully compare with observed flight test data. However, caution is recommended in interpreting these results, as 12.5% is likely an unreasonably high porosity for metals. Real metals, such as those used in flight tests, may have near-zero porosity. Other sources for interfaces, such as inclusions and dislocations, should also be considered.

Acknowledgements

The authors wish to thank Torch Technologies for supporting this work as part of their micro-debris characterization study. This paper describes objective technical results and analysis. Any subjective views or opinions that might be expressed in the paper do not necessarily represent the views of the U.S. Department of Energy or the United States Government. Sandia National Laboratories is a multimission laboratory managed and operated by National Technology & Engineering Solutions of Sandia, LLC, a wholly owned subsidiary of Honeywell International Inc., for the U.S. Department of Energy's National Nuclear Security Administration under contract DE-NA0003525.

References

[1] McGlaun, J.M., Thompson, S.L., Elrick, M.G., 1990. CTH: A Three-Dimensional Shock Wave Physics Code, International Journal of Impact Engineering, 10(1-4), pp. 351-360.

[2] Hertel, E.S. Bell, R.L., Elrick, M.G., Farnsworth, A.V., Kerley, G.I., McGlaun, J.M., Petney, S.V., Silling, S.A., Taylor, P.A., Yarrington, L., 1993. "CTH: A Software Family for Multi-Dimensional Shock Physics Analysis," Proceedings of the 19th International Symposium on Shock Waves, pp. 377-382.

[3] Grain Size in Pure Aluminum, Image Analysis Report 262, Clemex, May 2013.

[4] Nakai, M., Itoh, G., 2014. The Effect of Microstructure on Mechanical Properties of Forged 6061 Aluminum Alloy, Materials Transactions 55, pp. 114-119.

[5] Johnson, G.R., Cook, W.H., 1983. "A Constitutive Model and Data for Metals Subjected to Large Strains, High Strain Rates and High Temperatures," Seventh International Symposium on Ballistics, The Hague, Netherlands.

[6] Silling, S.A., 1996. "CTH Reference Manual: Viscoplastic Models," SAND91-0292, Sandia National Laboratories, Albuquerque, NM.

[7] Schmitt, R.G., Crawford, D.A., Harstad, E.N., Hensinger, D.M., Ruggirello, K.P., 2017. "CTH User's Manual and Input Instructions, Version 12.0," Sandia National Laboratories, Albuquerque, NM.